N-Phenyl-2-Pyridone-Derived Endoperoxide Exhibiting Dual Activity by Suppressing both Lung Cancer and Idiopathic Pulmonary Fibrosis

Lei Wang, Hao Wu, Ziang Liu, Yanping Li, Yu Si, Rensong Sun, Yun Nie, Yuan Qiao, Xiao Qian, Shengli Zhang, Wen Sun, Yue Pan,* and Engin U. Akkaya**

State Key Laboratory of Fine Chemicals, Department of Pharmaceutical Engineering, Dalian University of Technology, 2 Linggong Road, 116024 Dalian (China). E-mail: leiwang@dlut.edu.cn (L.W.); panyue0811@dlut.edu.cn (Y.P.); eua@dlut.edu.cn (E.U.A.).

Conventional light-driven photodynamic therapy (PDT) to generate toxic singlet oxygen are potential for cancer therapeutics but limited by the light penetrability and hypoxia tumor. PDT-involved combinational therapy could enhance overall therapeutic effects and reduce drug resistance, while disadvantages such as diverse pharmacokinetics among different ingredients, low active-ingredient loading, inevitably utilization of non-functional components need to be addressed. Here we report an endoperoxide ***E5*** *synthesized via 'in vitro' PDT could spontaneously deliver singlet oxygen, triplet oxygen and 3-methyl-N-phenyl-2-pyridone as an analogue of pirfenidone (Approved drug for treatment of idiopathic pulmonary fibrosis), showing great potential for treating non-small cell lung cancer and idiopathic pulmonary fibrosis. In aqueous solution,* ***E5*** *could undergo a clear cycloreversion to afford three components with a half-life time of 8.3 hours and it efficiently suppress the migration and invasion of lung cancer cell as well as*

*the TGF-β1 induced fibrosis in vitro. In vivo experiments suggest that **E5** not only efficiently inhibits tumor growth, decreases the HIF-1α protein levels, relieves idiopathic pulmonary fibrosis, but shows good biocompatibility. Many evidence reveal that both singlet oxygen and 3-methyl-N-phenyl-2-pyridone are therapeutic ingredients, and triplet oxygen could relieve tumor hypoxia which is an inevitable issue in conventional PDT. Our study validates that endoperoxides as single active components containing multiple ingredients including singlet oxygen are of exceptionally therapeutic potential.*

Cancers are one of the major disease threatening to the lives of human beings for centuries[1]. Photodynamic therapy (PDT)[2-4], a strategy based on the photochemical generation of cytotoxic singlet oxygen ($^1O_2$)[5] through the intermediacy of a photosensitizer has been considered a promising therapeutic technique for many cancers. Compared to conventional therapies, PDT not only leads to the minimization of systemic toxicity, but could activate the immune response and block tumor angiogenesis[6-7]. Apart from acting as a monotherapy, PDT could be integrated with chemotherapy for enhancing overall therapeutic effects and reducing drug resistance. However, application of PDT is limited by relatively low tissue penetration ability of light[8] and tumor hypoxia[9], which restricts the photosensitized generation of singlet oxygen. Meanwhile, current PDT-involved combinational therapy mainly relay on the encapsulation of photosensitizers and chemical drugs with a carrier generally challenged by the diverse pharmacokinetics among different ingredients, low active-ingredient loading and inevitably utilization of low-biocompatible or non-functional components[3-4].

Very recently, our group[10-12] and others[13-15] proved that endoperoxides, singlet oxygen carriers constructed by photosensitization *in vitro*, were potential anticancer agents which could self-deliver singlet oxygen to tumor through cycloreversion without the participation of light and

tumor oxygen. Meanwhile, many endoperoxides could release certain amount of triplet oxygen[16-17] which is likely to increase tumor oxygenation thus reversing hypoxic tumor programming[18-19]. Thus, we conjecture that a judicious design of endoperoxide could produce single active component delivering singlet oxygen, triplet oxygen and other therapeutic ingredient for synergistic treatment of cancer as long as cancer combined disease. In this Article, we present an endoperoxide **E5** undergoes clean cycloreversion reaction to release singlet oxygen, triplet oxygen and 3-methyl-N-phenyl-2-pyridone, showing great potential for treating non-small cell lung cancer (NSCLC)[20] and idiopathic pulmonary fibrosis (IPF)[21-22], two malignant lung disease sharing similar characteristics such as increased proliferation rates and epithelial mesenchymal transition (EMT)[23-25], but both are incurable.

Results and discussion

Design, synthesis, characterization and preliminary test

To date, many endoperoxides could deliver singlet oxygen but their precursors (naphthalene, anthracene or 2-pyridone) have no therapeutic effect, which driving us to design a medicative precursor. Pirfenidone (5-methyl-N-phenyl-2-pyridone, **P3**) is an FDA-approved drug[26-27] for idiopathic pulmonary fibrosis and its analogues (6-methyl-N-phenyl-2-pyridone **P2**, 4-methyl-N-phenyl-2-pyridone **P4**, 3-methyl-N-phenyl-2-pyridone **P5**, Supplementary Fig. 1) are all reported to present potential to relief fibrotic lesions[28-29]. Very recently, many evidences revealed that pirfenidone showed anti-cancer ability for NSCLC and pancreatic cancer[30-32]. Thus, we reasoned that pirfenidone or N-phenyl-2-pyridone-derived endoperoxide could be designed as single active component, and the released singlet oxygen and N-phenyl-2-pyridone will contribute to anti-cancer and anti-IPF effect. We first synthesized five *N*-phenyl-2-pyridone analogues with different methyl substitution patterns (Supplementary Fig. 1) and all compounds were obtained in good to

excellent yields (71 to 93%) except of **P2**, a 6-methyl substituted pyridone was isolated in 13% yield. Upon a methylene blue-mediated photochemical reaction[33], various endoperoxides as singlet oxygen-containing multicomponent agents were readily obtained (Fig. 1b). The clean cycloreversion and efficient release of singlet oxygen in aqueous environment are critical capability of endoperoxides for biology study, which drive us to study the cycloreversion of endoperoxides in aqueous solution via ^{1}H NMR analysis first (Fig. 1c, Supplementary Fig. 2-4). The results suggested that **E2**, **E3** and **E4** partly decomposed in aqueous solution resulting complex mixtures rather than undergoing clean cycloreversion. Instead, **E5**, a 3-methyl substituted 2-pyridone endoperoxide underwent clear cycloreversion to afford its synthetic precursor **P5** with a half-life as 8.3 hours (Supplementary Fig. 5). Its half-life time measured in organic solvent is 42.3 hours, five-fold than that in aqueous phase (Supplementary Fig. 6). Meanwhile, singlet oxygen trapping study using SOSG, a commonly used singlet oxygen probe in aqueous solution suggested that **E5** could efficiently release singlet oxygen (Fig. 1d). The efficiently release of singlet oxygen from **E5** was further confirmed using another singlet oxygen probe DPBF in organic environment (Fig. 1e). Next, an optical oxygen sensor was applied to directly detect the released oxygen from **E5**. As expected, dissolved oxygen was significantly increased to 32 mg/ml after the addition of endoperoxide **E5** suggesting the effectively produced oxygen (Fig. 1f). To further investigate the generation of singlet oxygen, tetramethylethylene (TME)[34], a singlet oxygen trapper was incubated with **E5** at 37 °C. By integrating specific peaks of the generated hydroperoxide **A** and **P5** in the ^{1}H NMR spectra, we were able to determine that approximately 50% singlet oxygen and 50% triplet oxygen were released simultaneously (Fig. 1g). Noteworthy, solid samples of endoperoxide **E5** can be stored in refrigerator for more than two years without detectable decomposition and its

melting point is 91-94 °C. Together, **E5** as a single active component could efficiently release singlet oxygen, triplet oxygen and 3-methyl-N-phenyl-2-pyridone in aqueous environment.

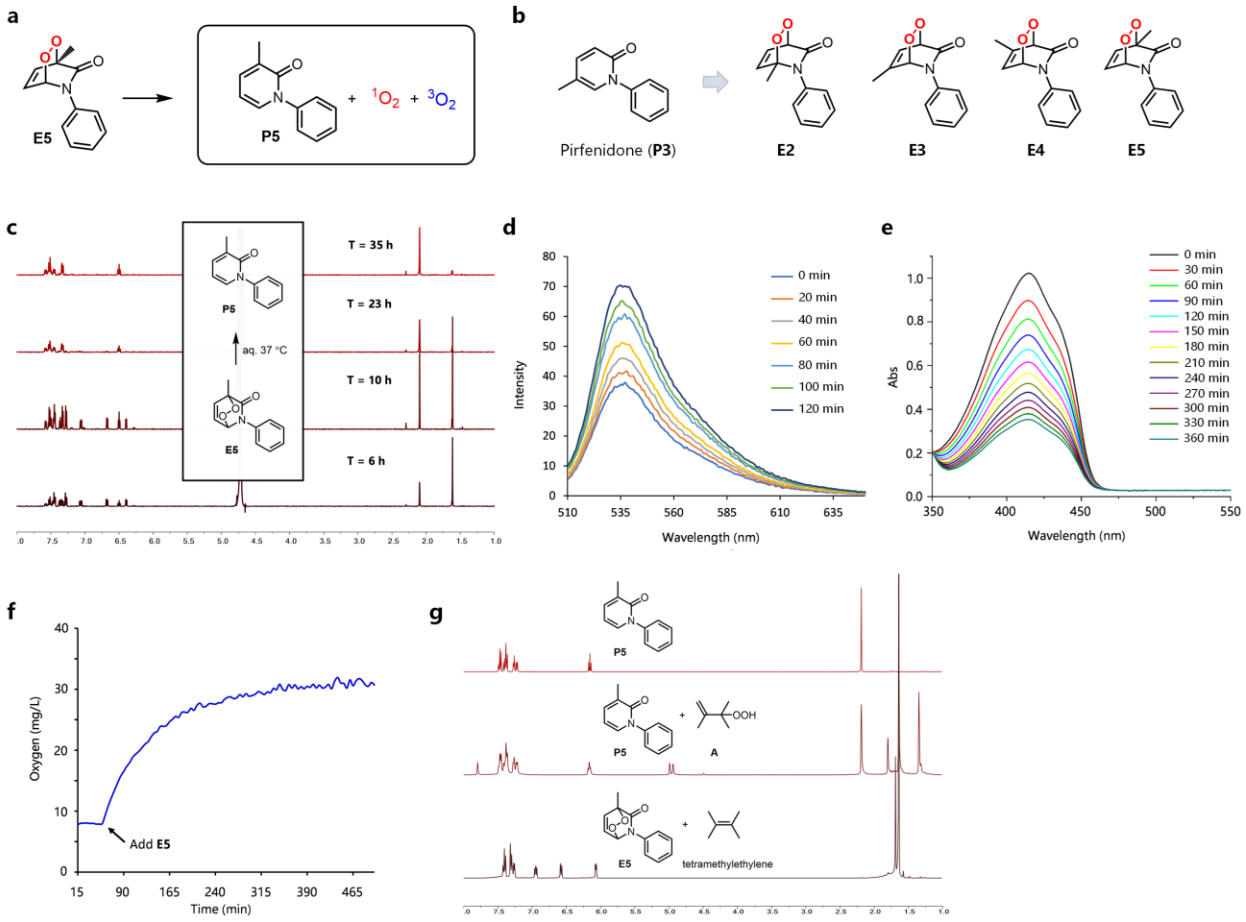

Fig. 1 Cycloreversion of E5 and the delivery of 3-methyl-N-phenyl-2-pyridone and singlet oxygen. a, Schematic for cycloreversion of **E5** to produce multifunctional agents. **b**, Pirfenidone and endoperoxides designed in this work. **c**, ^{1}H NMR spectra of **E5** in D_2O at 37 °C for different times. **d**, Singlet oxygen detection of **E5** (375 μM) using SOSG (12.5 μM) in PBS buffer at 37 °C. **e**, Singlet oxygen detection of **E5** (750 μM) using DPBF (37.5 μM) in DMF at 37 °C. **f**, Oxygen release from **E5** (20 mM in PBS buffer) at 37 °C was detected by a dissolved oxygen meter. **g**, Singlet oxygen trapping using tetramethylethylene (1-1 ratio to **E5**) in $CDCl_3$.

Anti-lung cancer ability *in vitro* and *in vivo*

With endoperoxide **E5** in hand, we first assessed its cytotoxic activity toward lung cancer cell. NCI-H1299 and A549 cells, two commonly used non-small cell lung cancer cell lines were incubated with **E5**, and the MTT (3-(4,5-dimethylthiazol-2-yl)-2,5-diphenyl tetrazolium bromide) assays displayed a dose-dependent cytotoxicity with IC_{50} of 44 and 119 μM, respectively (Fig. 2a and 2b). In addition, three other cancer cell lines (Hela, SK-OV-3 and HepG2) and non-tumorigenic cell lines HUVEC were tested and **E5** showed moderate cytotoxicity against cancer cells with good selectivity to HUVEC (Fig. 2c, Supplementary Fig. 7-10). Uptake into the cells and intracellular release of $^1O_2$ is crucial for effective therapeutic action of endoperoxides. 2',7'-Dichlorodihydrofluorescein diacetate (DCFH-DA) is a nonpolar dye which can be converted into nonfluorescent DCFH by cellular esterases, but transformed into highly fluorescent DCF by a reaction with intracellular reactive oxygen species. The resulting oxidatively stressed cells showed strong green fluorescence, signaling the release of $^1O_2$ from **E5**, whereas control cells treated with **P5** show negligible fluorescence (Fig. 2d). A cell-based wound healing assay showed that **E5** could significantly prevent A549 cells moving to close up the wound (**E5**: 21%, control: 60%), suggesting its capability of inhibiting cellular migration *in vitro* (Fig. 2e). Meanwhile, transwell invasion assay was designed and the result strongly suggested the inhibitory activity of **E5** to cancer cell invasion (Fig. 2f). To be noted, **P5** an important ingredient from **E5** was used as control and many evidences suggested that it provided anticancer ability in agreement with pirfenidone[30] (Fig. 2e, Supplementary Fig. 11). Next, we aimed to distinguish different stages of cell apoptosis caused by **E5** using FITC-labeled Annexin V/propidium iodide (PI) staining. Annexin V staining indicates the loss of membrane integrity which accompany early stage of cell death resulting from apoptotic or necrotic processes, while PI can only stain the nucleus of late apoptotic or dead cells through the damaged cell membrane. As shown in Fig. 2g, negligible green and red fluorescence

were found when cells were incubated with **P5**. While, significant green and red fluorescence were observed from **E5** incubated cells, indicating the late apoptotic stage of cells. Meanwhile, the dead and live cells were distinguished by Calcein acetoxymethylester (Calcein-AM) and PI co-staining (Fig. 2h) and **E5** group caused much higher cell-death rates (red fluorescence).

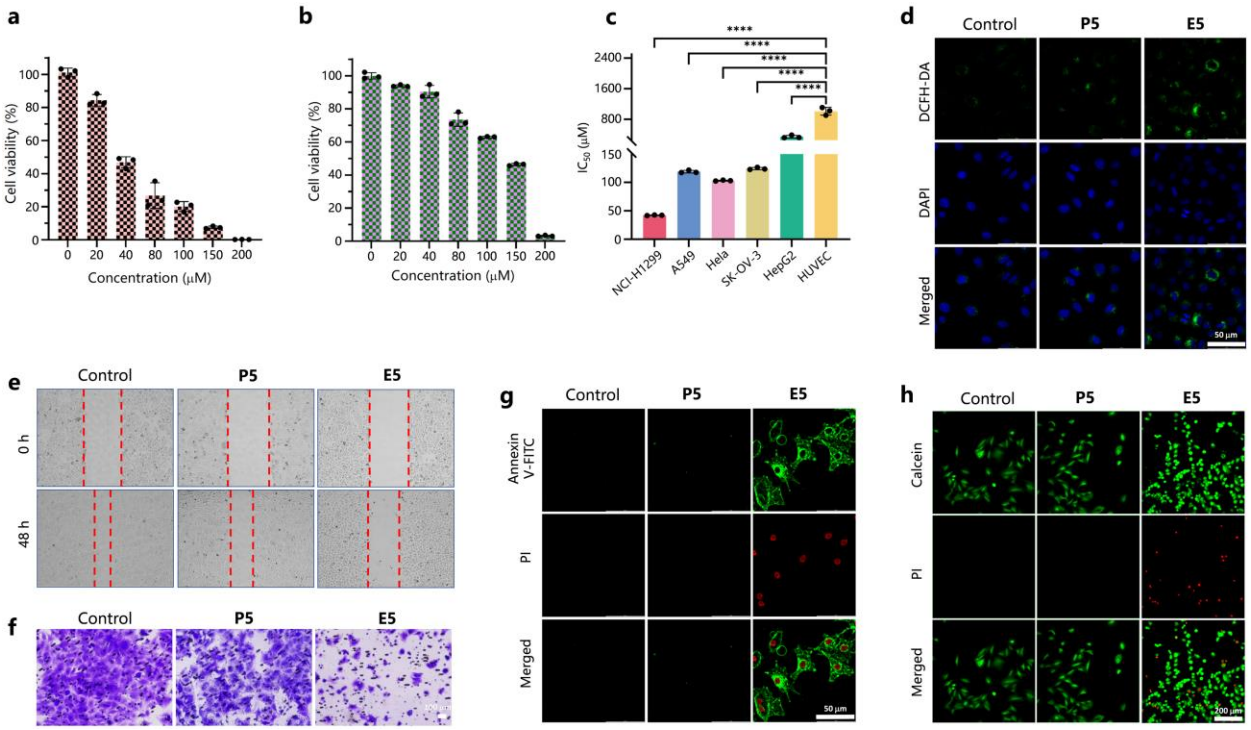

Fig. 2 In vitro anti-lung cancer properties of E5. a, Cell viability of NCI-H1299 cell treated with **E5** at various concentrations (0, 20, 40, 80, 100, 150, 200 μM). **b,** Cell viability of A549 cell treated with **E5** at various concentrations (0, 20, 40, 80, 100, 150, 200 μM). **c,** IC_{50} of **E5** toward different cell lines. **d,** Intracellular singlet oxygen detection of **E5** (40 μM) using DCFH-DA (10 μM) in A549 cells. **P5** (40 μM) was used as a control. **e,** Wound healing assay of A549 cells under different treatments (**E5** or **P5**, 100 μM). **f,** Transwell invasion assay of A549 cells under different treatments (**E5** or **P5**, 100 μM). **g,** Fluorescence imaging of Annexin V-FITC and PI stained A549 cells in different groups (**E5** or **P5**, 160 μM). **h,** Fluorescence imaging of Calcein-AM and PI stained A549 cells in different groups (**E5** or **P5**, 200 μM).

On the basis of its promising anti-tumor activity *in vitro*, we further studied the feasibility of **E5** as a therapeutic agent using A549 xenograft model developed in BALB/c mice. When the tumor volume reached to 50 mm^3 approximately, mice were randomly divided into three groups

(control, **P5** and **E5**). Mice in control group were administrated with 0.5% CMC-Na by intragastric injection, and mice in **E5** and **P5** group were administrated with indicated compounds for every other day (300 mg/kg). Throughout two weeks of treatment, tumor volume and body weight of each mouse was recorded and all mice kept their body weight and behaved normally, suggesting the high biocompatibility of **E5** (Fig. 3b**)**. As shown in Fig. 3c-3e, the tumor volume and tumor weight after **E5** treatment decreased by 86% and 65%, respectively. Meanwhile, **P5** treatment resulted in 29% and 33% decreasing in tumor volume and the tumor weight, compatible with its inhibitory ability *in vitro* experiment. Furthermore, the histological analysis was conducted by staining tumor tissues using H&E, Ki-67, TdT-mediated dUTP nick-end labeling (TUNEL), and significant damage including chromatic agglutination and karyopyknosis was noticed in **E5** group, suggesting its good anticancer activity (Fig. 3f and 3g**)**. Hypoxia is one of the main characteristics of solid tumors which are mainly mediated by hypoxia-inducible factor (HIF)[35] and many studies have shown that there is a close relationship between overexpressed HIF-1α driven by intratumoral hypoxia and increased patient mortality. Unlike PDT that worsens hypoxia through oxygen consumption and vascular shutdown effects[36], endoperoxides could not only release singlet oxygen without the consumption of tumor oxygen, but also deliver triplet oxygen to tumor. In the pilot study, we determined that **E5** could release 50% triplet oxygen during the cycloaddition reaction (*vide supra*), which inspired us to study the hypoxia relief ability of **E5** *in vivo*. As expected, immunofluorescence analysis of HIF-1α on tumor tissue suggested that **E5** could remarkably decrease the HIF-1α protein levels (Fig. 3g). To further evaluate the biocompatibility of **E5** *in vivo*, blood samples and the major organs of mice were tested for hematological and histological analysis, and no remarkable physiological damage was observed (Supplementary Fig. 13-14).

Together, **E5** was proved as a promising multicomponent carrier with good anti-lung cancer effects and excellent biosafety in living animals.

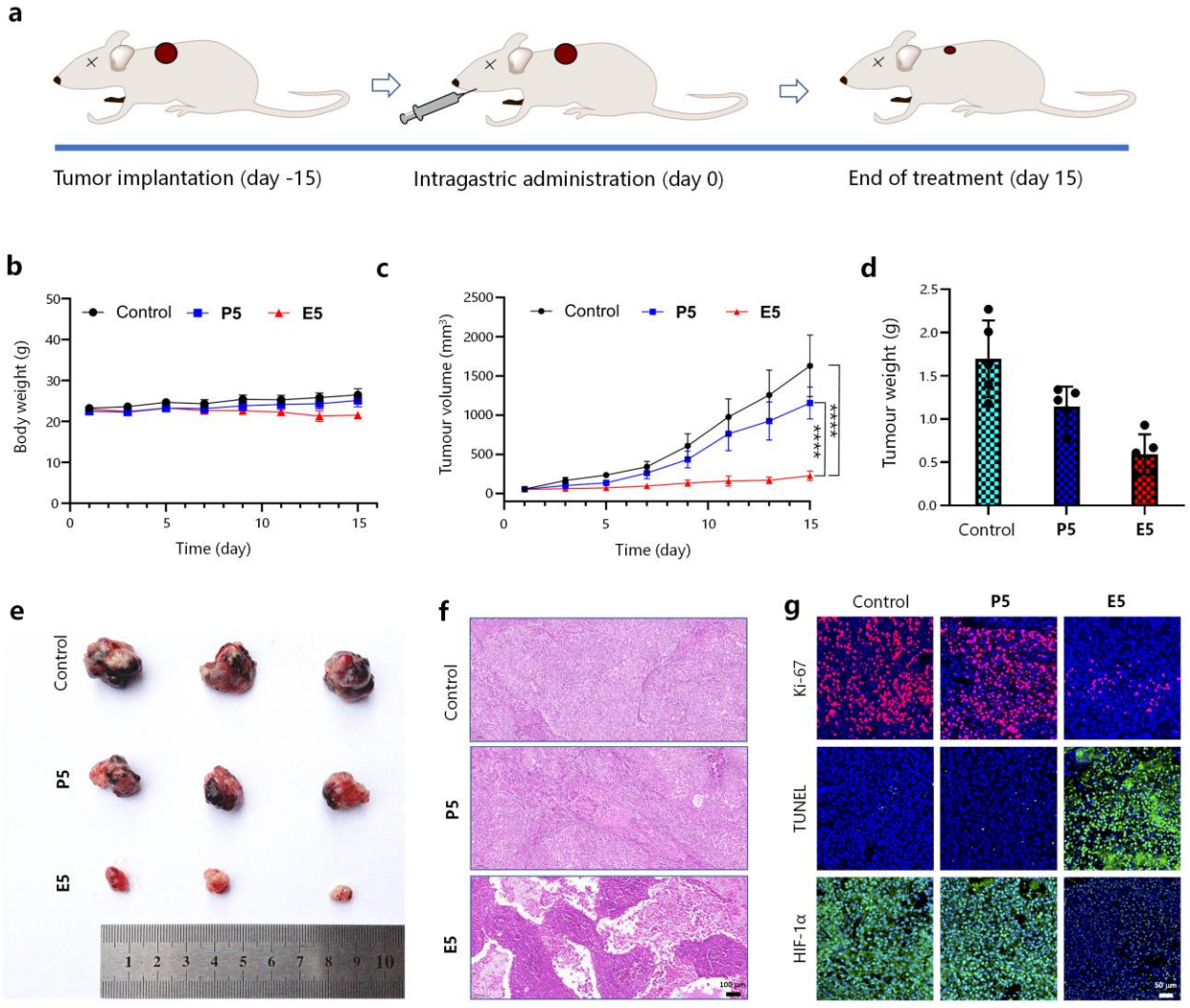

Fig 3 *In vivo* anti-lung cancer properties of E5. a, Schematic for *in vivo* anti-lung cancer study. **b,** Time evolution of mouse weight under different treatments. **c,** A549 tumor growth inhibition in different groups. **d,** A549 tumor weight under different treatments. The data present means ± s.d. of five replicates. **e,** Representative tumor images after different treatments. **f,** H&E staining of tumor sections after different treatments. **g,** Ki-67, TUNEL and HIF-1α immunofluorescence staining of tumor sections after different treatments. (Control: 0.5 % CMC-Na, **P5**: 300 mg/kg of **P5** in 0.5 % CMC-Na, **E5**: 300 mg/kg of **E5** in 0.5 % CMC-Na)

Anti-idiopathic pulmonary fibrosis study *in vitro* and *in vivo*

Having confirmed the anti-lung cancer potential of **E5**, we next evaluated its therapeutical effect for IPF which features pathological findings including fibroblast migration, proliferation, epithelial mesenchymal transition (EMT)[37-38]. Initially, we assessed the anti-fibrosis ability of **E5** *in vitro* using IMR-90 cell line[38] induced by transforming growth factor β1 (TGF-β1), a crucial profibrotic factor in lung fibrosis which can enhance the expression of fibrosis marker α-SMA. Immunofluorescence study showed that TGF-β1 significantly increased the expression of α-SMA, demonstrating a successful myofibroblast transformation (Fig. 4a). With the treatment of pirfenidone, **P5** and **E5**, expression of α-SMA in IMR-90 cell line was clearly inhibited, suggesting their inhibition differentiation potential especially **E5**. Meanwhile, inhibitory activity of singlet oxygen was determined using a methylene blue (MB)-mediated photosensitized reaction and the results clearly showed that singlet oxygen could inhibit the expression of α-SMA[39]. Transwell migration assay was designed to evaluate the migration of cells with various treatments (Fig. 4b, Supplementary Fig. 15). The number of cells passing through the ependyma of the transwell in the **E5** group were lower than pirfenidone, **P5** and MB-mediated groups, strongly confirming the inhibitory potential of **E5** for proliferation and migration. Similar functional superiorities were observed in a wound healing assay and the number of migrated cells were significantly decreased when cells were treated with **E5** (Supplementary Fig. 16). Next, EMT related proteins were analyzed by western blot (WB) and the result showed that TGF-β1 downregulated the expression of epithelial marker E-cadherin (20% to control) but upregulate N-cadherin, Vimentin and Twist (234%, 566%, and 245% to control, respectively, Fig. 4c-4g)[40]. Pirfenidone significantly upregulate the expression of E-cadherin and downregulated N-cadherin, Vimentin and Twist, suggesting it relieved pulmonary fibrosis *via* an EMT-related process. **P5** and MB-mediated

groups exhibited similar tendency, but better therapeutic potential compared to pirfenidone group. Compared to pirfenidone, **E5** showed better regulating ability, either in promoting E-cadherin (185% to model) or inhibiting N-cadherin, Vimentin and Twist (64%, 40%, and 53% to model, respectively). In addition, TGF-β1 induced EMT with cancer cell A549 was established[41], and the transwell migration and wound healing assay both confirmed exciting inhibitory ability of **E5** *in vitro* (Supplementary Fig. 17-18). Together, **E5** significantly inhibited the proliferation of fibroblasts and regulated the expression of fibrosis markers including α-SMA, E-cadherin, N-cadherin, Vimentin and Twist, demonstrating its potential anti-IPF ability. In view of above-mentioned results, we can deduce that components released from **E5** work together for the relief of IPF, especially singlet oxygen and **P5**.

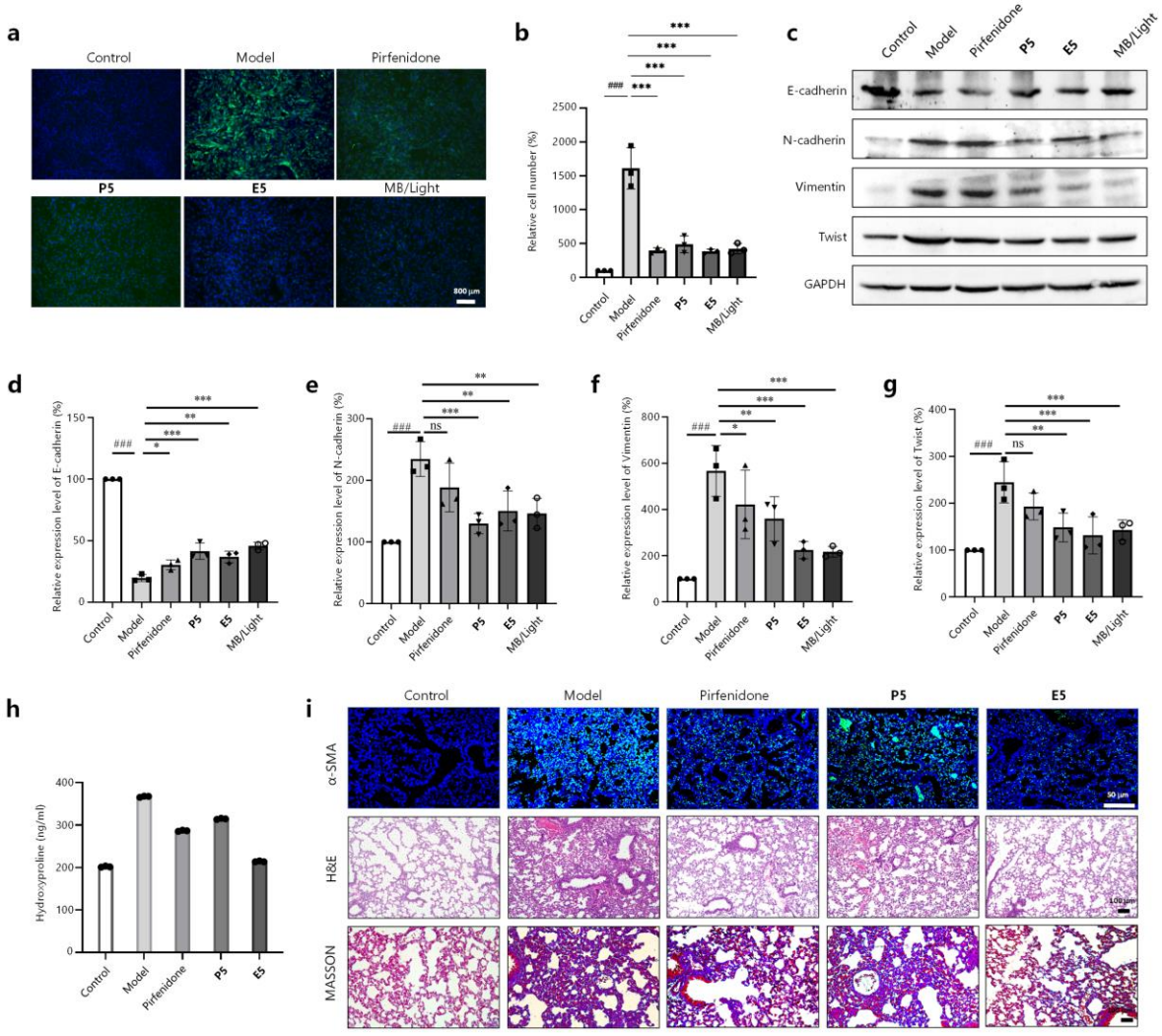

Fig 4 In vitro Anti-IPF study. a, α-SMA immunofluorescence staining of TGF-β1 induced IMR-90 cell line under different treatments. **b,** Transwell migration assay of TGF-β1 induced IMR-90 cell line under different treatments. **c,** Expression level of EMT-related markers of TGF-β1 induced IMR-90 cell line under different treatments. Relative expression of E-cadherin (**d**), N-cadherin (**e**), Vimentin (**f**) and Twist (**g**). Control: IMR-90 cells without any treatment, Model: IMR-90 cells were treated with TGF-β1 (5 ng/mL), Pirfenidone: TGF-β1 (5 ng/mL) induced IMR-90 cells were treated with Pirfenidone (80 μM), **P5**: TGF-β1 (5 ng/mL) induced IMR-90 cells were treated with **P5** (80 μM), **E5**: TGF-β1 (5 ng/mL) induced IMR-90 cells were treated with **E5** (80 μM), MB/light: TGF-β1 (5 ng/mL) induced IMR-90 cells were treated with methylene blue (17.5 μM) with 625 nm LED for 20 min. The data present means ± s.d. of three replicates. **h,** Quantitative of hydroxyproline in bleomycin (BLM)-induced IPF mice. **i,** α-SMA, H&E and Masson staining of the lung of mice after different treatments.

The excellent ability of **E5** for *in vitro* anti-IPF encouraged us to further investigate whether it can alleviate pulmonary fibrosis *in vivo*. Lung fibrosis of mice induced by bleomycin (BLM) is the most commonly used preclinical model for IPF studies,[42] and we established the model of BLM-induced lung fibrosis using C57BL/6 mice, which were exposed to four groups randomly: model, pirfenidone, **P5** and **E5** group by intragastric administration once a day. After 16 days of treatments, all mice kept their body weight and lung index (the ratio of lung weight to body weight), suggesting good safety of pirfenidone, **P5** and **E5** (Supplementary Fig. 19-20). To study the relief of collagen deposition, hydroxyproline (HYP)[43], an important biomarker for evaluating idiopathic pulmonary fibrosis was measured first. Obviously, bleomycin significantly increased the hydroxyproline level as compared to non-IPF controls (175%), indicative of increased deposition of collagen in the lung (Fig. 4h). Treatment with pirfenidone and **P5**, given once a day starting at the stage of established fibrosis led to a significant decrease in hydroxyproline levels (80% and 88% to model, respectively). Most importantly, **E5** administration significantly reduced hydroxyproline to the same level as the control group (60% to model, 106% to control), suggesting its exceptional anti-pulmonary fibrosis potential. Meanwhile, expression of TGF-β1 in each group were investigated (Supplementary Fig. 21), and it showed that **E5** clearly suppressed the TGF-β1 expression[44], suggesting TGF-β1 signaling is involved in the attenuation of fibrosis by endoperoxide **E5**. It should be noted that **P5** can inhibit the expression of TGF-β1 as well. As shown in Fig. 5i, α-SMA[45], marker of myofibroblast differentiation was dramatically increased in the lung sections of the BLM group, but decreased significantly with the treatment pirfenidone and **P5**. To our delight, α-SMA expression in **E5** group was remarkably reduced suggesting that **E5** owns superior ability to inhibit the activation of myofibroblasts and to rebuild the lung architecture.

Morphologically, the lungs from the control group of mice showed normal pulmonary architecture and tissue structure, but BLM treated mice exhibited increased histological evidence of fibrosis (Fig. 5i). By contrast, in the pirfenidone and **P5** group, collagen deposition was significantly decreased, and architectural structure was improved. Most importantly, pulmonary fibrosis and collagen deposition were further decreased in **E5** group, suggesting its greater potential for anti-IPF. Masson trichrome staining imparts a blue color to collagen fibers, which were found in disease model, pirfenidone and **P5** groups (Fig. 5i). Obviously, less blue area staining of collagen was found in **E5** group, presenting visual evidence for **E5** recovery of the alveolar structure and efficient alleviation of IPF. In addition, the heatmap plot highlights the expressed genes associated with EMT are affected by **E5** and **P5** (Supplementary Fig. 22), suggesting that the mechanism of antifibrosis of **E5** and **P5** group may be related to the inhibition of the EMT signaling pathway. Additional H&E staining of normal organs suggest the good biosafety of **E5** *in vivo* (Supplementary Fig. 23). All animal experiments described in this paper were approved by the local research ethics review board of the Animal Ethics Comittee of Dalian University of Technology, ethics approval no. is DUTSCE231229-01.

Conclusion

Single active components containing multiple therapeutic ingredients are promising for many malignant diseases as well as multi-diseases. Photodynamic therapy has been emerged as a powerful strategy for cancer therapeutics which not only shows the minimization of systemic toxicity, but could activate the immune response and block tumor angiogenesis. However, the generation of toxic singlet oxygen was limited by relatively low tissue penetration ability of light and tumor hypoxia. A combinational therapy of PDT and chemotherapy could enhance overall

therapeutic effects and reduce drug resistance. While, the diverse pharmacokinetics among different ingredients, low active-ingredient loading and inevitably utilization of low-biocompatible or non-functional components need to be addressed. Endoperoxides constructed via photosensitization *in vitro* could self-deliver singlet oxygen for cancer treatment without the participation of light and tumor oxygen. However, currently reported endoperoxides can only deliver singlet oxygen and their precursors have no therapeutic effect, which suggest the urgency to develop a single active endoperoxide for delivering multiple therapeutic ingredients, also in the context of singlet oxygen.

In this Article, we designed and synthesized an endoperoxide **E5** which could simultaneously deliver singlet oxygen, triplet oxygen and 3-methyl-N-phenyl-2-pyridone. 3-Methyl substituted phenyl-2-pyridone was proved as a good singlet oxygen carrier and the generated endoperoxide could deliver singlet oxygen and its precursor in excellent efficiency in aqueous environment. *In vitro* study showed that it could not only efficiently suppress the migration and invasion of lung cancer cell but inhibited the TGF-β1 induced myofibroblast differentiation. *In vivo* work suggested that the endoperoxide **E5** can efficiently inhibit the tumor growth and the expression of HIF-1α protein, and relieve bleomycin-induced pulmonary fibrosis with good biocompatibility. Many results reveal that both singlet oxygen and 3-methyl-N-phenyl-2-pyridone are therapeutic ingredients for two diseases, and the released triplet oxygen could possibly relieve tumor hypoxia. As a proof of concept, this study validates that endoperoxides as single active components containing multiple ingredients including singlet oxygen are of exceptionally therapeutic potential.

References

1. Siegel, R. L., Miller, K. D., Wagle, N. S., Jemal, A. Cancer statistics 2023. *CA Cancer J. Clin*. **73**, 17–48 (2023).
2. Pham, T. C. et al. Recent strategies to develop innovative photosensitizers for enhanced photodynamic therapy. *Chem. Rev*. **121**, 13454−13619 (2021).
3. Lucky, S. S., Soo, K. C., Zhang, Y. Nanoparticles in photodynamic therapy. *Chem. Rev*. **115**, 1990−2042 (2015).
4. Cheng. L. et al. Functional nanomaterials for phototherapies of cancer. *Chem. Rev*. **114**, 10869−10939 (2014).
5. Mascio, P. D. et al. Singlet molecular oxygen reactions with nucleic acids, lipids, and proteins. *Chem. Rev*. **119**, 2043−2086 (2019).
6. Spring, B. Q., Rizvi, I., Xu, N., Hasan, T. The role of photodynamic therapy in overcoming cancer drug resistance. *Photochem. Photobiol. Sci*. **14**, 1476−1491 (2015).
7. Castano, A. P., Mroz, P., Hamblin, M. R. Photodynamic therapy and anti-tumour immunity. *Nat. Rev. Cancer* **6**, 535−545 (2006).
8. Allison, R. R., Sibata, C. H. Oncologic photodynamic therapy photosensitizers: a clinical review. *Photodiagnosis Photodyn. Ther*. **7**, 61–75 (2010).
9. Wilson, W. R., Hay, M. P. Targeting hypoxia in cancer therapy. *Nature Reviews Cancer* **11**, 393–410 (2011).
10. Turan, I. S. et al. A bifunctional photosensitizer for enhanced fractional photodynamic therapy: singlet oxygen generation in the presence and absence of light. *Angew. Chem. Int. Ed*. **55**, 2875–2878 (2016).
11. Kolemen, S. et al. Remote-controlled release of singlet oxygen by the plasmonic heating of endoperoxide-modified gold nanorods: towards a paradigm change in photodynamic therapy. *Angew. Chem. Int. Ed*. **55**, 3606–3610 (2016).
12. Wu, H. et al. Targeted singlet oxygen delivery: a bioorthogonal metabolic shunt linking hypoxia to fast singlet oxygen release. *Angew. Chem. Int. Ed*. **61**, e202210249 (2022).
13. Li, G. et al. Photothermally responsive conjugated polymeric singlet oxygen carrier for phase change-controlled and sustainable phototherapy for hypoxic tumor. *Research* **2020**, 5351848 (2020).

14. Kuang, S. et al. Photodecaging of a mitochondria-localized iridium(III) endoperoxide Complex for two-photon photoactivated therapy under hypoxia. *J. Am. Chem. Soc*. **144**, 4091−4101 (2022).
15. Xiao, W. et al. 2-Pyridone-functionalized aza-BODIPY photosensitizer for imaging-guided sustainable phototherapy. *Biomaterials* **183**, 1–9 (2018).
16. Fudickar, W., Linker, T. Release of singlet oxygen from aromatic endoperoxides by chemical triggers. *Angew. Chem. Int. Ed*. **57**, 12971–12975 (2018).
17. Fudickar, W., Linker, T. Why triple bonds protect acenes from oxidation and decomposition. *J. Am. Chem. Soc*. **134**, 15071−15082 (2012).
18. Cheng, Y. et al. Perfluorocarbon nanoparticles enhance reactive oxygen levels and tumour growth inhibition in photodynamic therapy. *Nature Communications* **6**, 8785 (2015).
19. Song, X. et al. Ultrasound triggered tumor oxygenation with oxygen-shuttle nanoperfluorocarbon to overcome hypoxia-associated resistance in cancer therapies. *Nano Lett*. **16**, 6145−6153 (2016).
20. Herbst, R. S., Morgensztern, D., Boshoff, C. The biology and management of non-small cell lung cancer. *Nature* **553**, 446–454 (2018).
21. Lederer, D. J., Martinez, F. J. Idiopathic pulmonary fibrosis. *N. Engl. J. Med*. **378**, 1811–1823 (2018).
22. du Bois, R. M. Strategies for treating idiopathic pulmonary fibrosis. *Nat. Rev. Drug Discov*. **9**, 129–140 (2010).
23. Raghu, G., Amatto, V.C., Behr, J., Stowasser, S. Comorbidities in idiopathic pulmonary fibrosis patients: a systematic literature review. *Eur. Respir. J*. **46**, 1113–1130 (2015).
24. Vancheri, C. Common pathways in idiopathic pulmonary fibrosis and cancer. *Eur. Respir. Rev.* **22**, 265–272 (2013).
25. Wang, C., Yang, J. Mechanical forces: the missing link between idiopathic pulmonary fibrosis and lung cancer. *European Journal of Cell Biology* **101**, 151234 (2022).
26. George, P. M., Wells, A. U. Pirfenidone for the treatment of idiopathic pulmonary fibrosis. *Expert Rev. Clin. Pharmacol*. **10**, 483−491 (2017).
27. Kim, E. S., Keating G. M. Pirfenidone: a review of its use in idiopathic pulmonary fibrosis. *Drugs* **75**, 219–230 (2015).

28. Margolin, S. B. Compositions and methods for reparation and prevention of fibrotic lesions. US005716632A (1996).
29. Karl, K. et al. Compounds and methods for treating inflammatory and fibrotic disorders. US20090318455A1 (2009).
30. Fujiwara, A. et al. Pirfenidone plays a biphasic role in inhibition ofepithelial-mesenchymal transition in non-small cell lung cancer. *Lung Cancer* **106**, 8–16 (2017).
31. Kozono, S. et al. Pirfenidone inhibits pancreatic cancer desmoplasia by regulating stellate. *Cells. Cancer Res*. **73**, 2345–2356 (2013).
32. Gao, F. et al. Biodegradable, pH-sensitive hollow mesoporous organosilica nanoparticle (HMON) with controlled release of pirfenidone and ultrasound-target-microbubble-destruction (UTMD) for pancreatic cancer treatment. *Theranostics* **9**, 6002–6018 (2019).
33. Turro, N. J., Chow, M. F., Rigaudy, J. Mechanism of thermolysis of endoperoxides of aromatic compounds. Activation parameters, magnetic field, and magnetic isotope effects. *J. Am. Chem. Soc*. **103**, 7218–7224 (1981).
34. Matsumoto, M., Yamada, M., Watanabe, N. Reversible 1, 4-cycloaddition of singlet oxygen to N-substituted 2-pyridones: 1, 4-endoperoxide as a versatile chemical source of singlet oxygen. *Chem. Commun*. **2005**, 483–485 (2005).
35. Kung, A. L. et al. Suppression of tumor growth through disruption of hypoxia-inducible transcription. *Nature Medicine* **6**, 1335–1340 (2000).
36. Wang, W., Moriyama, L. T., Bagnato, V. S. Photodynamic therapy induced vascular damage: an overview of experimental PDT. *Laser Phys. Lett*. **10**, 023001–023008 (2013).
37. Kawashima, T. et al. Contrary effects of sphingosine-1-phosphate on expression of *α*-smooth muscle actin in transforming growth factor β1-stimulated lung fibroblasts. *European Journal of Pharmacology* **696**, 120–129 (2012).
38. Mou, Y. et al. Dopamine receptor agonists ameliorate bleomycin-induced pulmonary fibrosis by repressing fibroblast differentiation and proliferation. *Biomedicine & Pharmacotherapy* **139**, 111500 (2021).
39. Li. S. et al. The effect of ALA-PDT on reversing the activation of cancer-associated fibroblasts in cutaneous squamous cell carcinoma. *Photodiagnosis and Photodynamic Therapy* **27**, 234–240 (2019).

40. Huang, Y. Y. et al. Mangostanin derivatives as novel and orally active phosphodiesterase 4 inhibitors for the treatment of idiopathic pulmonary fibrosis with improved safety. *J. Med. Chem*. **64**, 13736−13751 (2021).
41. Liu, Y. et al. Competitive endogenous RNA is an intrinsic component of EMT regulatory circuits and modulates EMT. *Nature Communications* **10**, 1637 (2019).
42. Li. R. et al. Novel drug delivery systems and disease models for pulmonary fibrosis. *Journal of Controlled Release* **348**, 95–114 (2022).
43. Udenfriend, S. Formation of hydroxyproline in collagen, *Science* **152**, 1335–1340 (1966).
44. Cui, X. et al. Hematoporphyrin monomethyl ether-mediated photodynamic therapy inhibits the growth of keloid graft by promoting fibroblast apoptosis and reducing vessel formation. *Photochem. Photobiol. Sci*. **19**, 114 (2020).
45. Phan, S. H. The myofibroblast in pulmonary fibrosis, *Chest* **122**, 286S–289S (2002).

Methods

Synthesis of endoperoxides

Syntheses and characterizations of compounds are provided in Supplementary Information.

Cycloreversion of endoperoxides

Endoperoxide **E2**-**E5** (2 mg) was dissolved in D_2O (1 mL) at room temperature, after removing undissolved solid, the aqueous solution was incubated at 37 °C and ^1H NMR was measured at indicated time. Cycloreversion of endoperoxide was analyzed by the production of their previous analogues (**P2**-**P5**).

Detection of singlet oxygen and dissolved oxygen

Singlet oxygen sensor green (SOSG) and 1, 3-diphenylisobenzofuran (DPBF) were used as probes to detect singlet oxygen released from endoperoxide **E5** in aqueous and organic solution,

respectively. Briefly, **E5** in 20 uL of DMSO (375 μM, final concentration) and SOSG (12.5 μM, final concentration) were incubated in PBS buffer (pH = 7.4) at 37 °C under dark. Fluorescence measurements were done with a fluorescence spectroscopy under excitation at 504 nm and the intensity increasing at 530 nm indicate the generation of singlet oxygen in aqueous solution. Meanwhile, 750 μM of **E5** was mixed with DPBF (37.5 μM, final concentration) in DMF at 37 °C under dark, and the UV-Vis measurements were taken at indicated time. Absorbance decrease at 417 nm was monitored which revealing the release of singlet oxygen from endoperoxide.

Cytotoxicity

The cytotoxic profiles of **E5** were obtained via MTT assays. Cells (8000 cells per well for NCI-H1299 and A549, 5000 cells per well for Hela, HepG2, SK-OV-3 and HUVEC) were seeded into 96-well plates and incubated at 37 ℃ for 24 hours. Then, the cells were treated with culture medium containing **E5** with various concentrations (0, 20, 40, 80, 100, 150, 200 μM). After 24 h, the cells were treated with 0.5% MTT and further incubated at 37 ℃ for 4 h. After removal of the medium, 150 μL DMSO was added to dissolve the formazan crystals and the absorbance was measured at 570 nm with a microplate reader (SpectraMax i3x, MD). The cell viabilities of endoperoxide treated cells were normalized to the untreated cells. Meanwhile, cytotoxicity of **P5** toward A549 cell line was measure as well and IC_{50} were obtained *via* Graphpad 8.

Intracellular singlet oxygen detection

A549 cells (1.5×10^5 cells per dish) were cultured at 37 °C for 24 h, **E5** or **P5** (40 μM) was added to different dishes respectively and further incubated for 6 h at 37 °C. The culture medium was removed and the cells were washed with PBS. Then, the cells were treated with DCFH-DA (10 μM in DMEM) and incubated at 37 ℃. After 45 minutes, the solution was removed and the

cells were washed with PBS followed by staining with DAPI (10 μg/mL) for 15 min. The extra dye was washed with PBS and the imaging was done with a fluorescence microscope (Leica DMI8).

Apoptosis Imaging

A549 cells (1.5×10^5 cells per dish) were cultured at 37 °C for 24 h. Then, **E5** or **P5** (160 μM) were respectively added to different dishes and incubated for 9 h. Then, the culture medium was removed and the cells were washed with PBS followed with further staining with Annexin V-FITC/PI according to the kit instructions. The images were observed with a fluorescence microscope (Leica DMI8). Meanwhile, A549 cells (8000 cells per well) were cultured at 37 °C for 24 h. Then, **E5** or **P5** (200 μM) were added to different dishes respectively and incubated for 2 h. Then, the culture medium was replaced and the cells were washed with PBS followed with further staining with Calcein AM/PI according to the kit instructions. The images were observed with a High Content Imaging System.

In vivo anticancer experiment

All the animal experiments involved in this work were approved by the ethics committee of the Dalian University of Technology. Female BALB/c nude mice (6-weeks-old) were subcutaneously implanted with A549 cells (1×10^7). When the tumor volumes reached to ~50 mm^3, the mice were randomly divided into three groups (five mice in each group): Mice in the first group were administered intragastrically with 0.5 % CMC-Na (control group). Mice in the second group were administered intragastrically with **P5** in 0.5 % CMC-Na (**P5** group, 300 mg/kg). Mice in the third group were administered intragastrically with **E5** in 0.5 % CMC-Na (**E5** group, 300 mg/kg). The administration was gave on every other day in the following two weeks and the tumor volume

(V) was calculated according to the following formula: $V = L \times W^2/2$ by measuring the tumor length (L) and width (W) of each mouse. After 14 days, the mice were all sacrificed. Tumor and major organs were fixed with paraformaldehyde (10% vol/vol), sectioned into slices and analyzed via hematoxylin-eosin (H&E) and immunofluorescence (Ki-67, TUNEL and HIF-1α) staining. The blood of mice were collected to determine the side effect of treatment.

In vitro Anti-IPF study

TGF-β1 (5 ng/mL) induced MCR-90 cells were used for *in vitro* anti-IPF study and MCR-90 cells without any treatment was used as control.

Immunofluorescence assay: MCR-90 cells incubated for 24 hours, were washed with PBS and fixed with 4% paraformaldehyde for 30 min at room temperature. Then, TGF-β1 was added and the cells was further incubated for 6 hours. After the treatment by pirfenidone, **P5**, **E5**, (80 μM) or MB-mediated photoreaction (17.5 μM, 625 nm LED, 20 min), cells were washed with PBS, block with 1% FBS for 15 min, primary antibody α-SMA (1:200, ABclonal) was added and the cell was further incubated at 4 °C for 24 h. After wash with PBS, Alexa Fluor® 488 goat anti-rabbit secondary antibody (1:200, Proteintech) was added and the cell was incubated for 1 h. Cell nuclei were stained with DAPI (1:100, Aladdin) and the cells was washed by PBS before imaging with fluorescence microscope (Olympus IX71).

Transwell migration assay: MCR-90 cells seeded into the upper chamber were induced by TGF-β1 under different treatments (pirfenidone, **P5**, **E5** at 80 μM concentration or a MB-mediated photoreaction: 17.5 μM, 625 nm LED, 20 min) in DMEM medium containing 2% FBS. After 48 h incubation, the chambers were washed with PBS, fixed with 4% paraformaldehyde for 30 min and stained with 0.1% crystal violet dye solution at room temperature for 30 min. After rinsed by

PBS, the cells were scraped with a cotton swab and each chamber was air-dried and imaged using fluorescence microscope (Nikon Eclipse Ts2-FL).

Wound healing assay: MCR-90 cells were cultured in 6-well plates at 37 °C for 24 h. Then, 200 μL of pipette was used to scratch cell monolayers for creating a wound artificially. After washed with PBS and replaced with fresh medium, TGF-β1 was added and the cells was further incubated for 6 hours. After the treatment by pirfenidone, **P5**, **E5** (80 μM) or MB-mediated photoreaction (17.5 μM, 625 nm LED, 20 min), the cells was further incubated for 48 h. Cells migrating from the edge of the wound were photographed at 0 and 48 h time points by fluorescence microscope (Olympus IX71).

Western blotting assay: MCR-90 cells were treated with TGF-β1 for 6 hours. After the treatment by pirfenidone, **E5**, **P5** (80 μM) or MB-mediated PDT (17.5 μM, 625 nm LED, 20 min), the cells were washed with ice-cold PBS and lysed in RIPA lysis buffer. Extracted total protein was homogenized in RIPA lysis buffer with protease inhibitor and quantified using a BCA protein assay kit (Shanghai EpiZyme Biotechnology Co., Ltd.). After denaturation, protein samples were then transferred to a PVDF membrane after gel electrophoresis using 8% SDS-PAGE and the membrane was blocked with TBST buffer containing 5% non-fat milk. After wash by TBST buffer, PVDF membrane was treated with different primary antibodies: N-Cadherin (1:1000), E-Cadherin (1:1000), Vimentin (1:1,000), Twist (1:1000) (all from Cell Signaling Technologies, Danvers, MA), and GAPDH (1:5000, Sigma-Aldrich) at 4 °C overnight. Then, the membranes were incubated with HRP-conjugated secondary antibodies at room temperature for 1 h. After wash with TBST, the protein bands were detected using enhanced chemiluminescent reagents (Solarbio Life Science, Beijing, China). The images were analyzed using Image J software and the results were normalized to GAPDH.

In vivo anti-IPF evaluation

After three days habituation, C57BL/6 mice (4-5 weeks old) were randomly assigned into five groups: control group, model group, pirfenidone group, **P5** group, and **E5**. The control group was treated with normal saline and the others were treated with bleomycin (BLM) by intratracheal instillation (2 mg/ml). The treatments began in the third day with 0.5% CMC-Na (control, model group), pirfenidone, **P5** or **E5** (400 mg/kg, in 0.5% CMC-Na solution) and mice weight were recorded throughout the treatment. After 16 days treatment, the rats were anesthetized by injection of pentobarbital sodium, and lung and other major organs were harvested after the mice were euthanized. The tissues were immersed in 4% formaldehyde solution at room temperature, lung section were subjected to H&E, Masson's and immunofluorescence staining and other organs were subjected to H&E staining.

Acknowledgements

This work was supported by the National Natural Science Foundation of China (22007008, 22178048), the LiaoNing Revitalization Talents Program (XLYC1902001, XLYC1907021) and the Fundamental Research Funds for the Central Universities (DUT23YG120, DUT19RC(3)009).